Barbara Bong[1,2]
Wassja A. Kopp[3]
Thomas Nevolianis[3]
Chalachew Mebrahtu[1,2]
Kai Leonhard[3]
Regina Palkovits[1,2,*]

Reaction Equilibria in the Hydrogen Loading and Release of the LOHC System Benzyltoluene/Perhydro Benzyltoluene

Liquid organic hydrogen carriers (LOHCs) can store and transport hydrogen by chemical bonding. Benzyltoluene (H0-BT) is an attractive LOHC that can take up 12 H per carrier molecule. The chemical equilibrium favors hydrogenation at lower temperatures and higher pressures. In this work, we study hydrogenation kinetics at 125–200 °C and 0.3–30 bar H_2. We perform ab initio calculations of all isomers of H0-BT and its (partially) hydrogenated forms to compute chemical equilibrium compositions. Despite hydrogenation being exothermic, full hydrogenation is thermodynamically possible almost up to the boiling temperature of the LOHC. Based on the obtained results, the tradeoff between the degree of hydrogenation and reducing the operating temperature is discussed.

Supporting Information available online

Keywords: Chemical energy storage, Chemical equilibrium constants, Kinetics, Liquid organic hydrogen carriers

Received: June 14, 2024; *revised:* January 28, 2025; *accepted:* January 29, 2025

DOI: 10.1002/ceat.12002

1 Introduction

For sustainable and stable energy supply, green hydrogen is highly attractive as a flexible energy carrier [1–7]. To successfully integrate hydrogen into energy systems, substantial volumes of hydrogen must be stored under limited spaces and transported over long distances. Additionally, strong requirements regarding the safety and usability of the hydrogen storage technology must be fulfilled [8]. A method for safe and easy hydrogen storage is provided by liquid organic hydrogen carriers (LOHCs): Hydrogen is loaded on the hydrogen-lean carrier compound ($LOHC^-$) in a catalytic hydrogenation reaction, resulting in covalent bonds between hydrogen and the carrier. In this way, hydrogen can be stored for a long time without self-discharge [1, 7, 9, 10]. Furthermore, the hydrogen-rich $LOHC^+$ can be transported via the established infrastructure under ambient conditions as the properties are similar to traditional fuels like diesel [4, 5, 11]. As soon as hydrogen is required, it is released in a catalytic dehydrogenation, and the unloaded $LOHC^-$ is reused [1, 4, 7]. For technical applications of the LOHC technology, benzyltoluene has been identified as a favorable LOHC system, as it is available on a technical scale and well characterized [4, 5, 12–15]. Furthermore, it shows highly attractive physicochemical properties like thermal robustness and low viscosity [4, 5, 12–14]. The loaded form of perhydro benzyltoluene (H12-BT) can store 12 hydrogen atoms per carrier molecule according to a formal storage capacity of 2.2 kWh hydrogen per kg of H12-BT (lower heating value) [16]. The loading of H0-BT is typically performed at temperatures between 150 °C and 300 °C and a hydrogen pressure of 30–50 bar [5, 12, 17]. To release the hydrogen from H12-BT, the reverse reaction is conducted at low pressures up to 5 bar or atmospheric conditions. While the hydrogenation is an exothermic reaction, the dehydrogenation is endothermic [12, 17, 18]. Hence, the thermodynamic equilibrium of these reactions should be shifted toward higher hydrogen loading by decreasing temperature or an increase of hydrogen partial pressure or total pressure according to Le Chatelier's principle [19–21]. Suitable catalysts for the loading of H0-BT and unloading of H12-BT are noble metals on oxides like platinum over aluminum or titanium oxide [5, 12, 17, 22]. For example, Rüde et al. [12] reported that hydrogen loading of at least 99.5 % could be obtained within 4 h using the established commercial catalyst S-Pt/Al_2O_3 (0.3 wt% Pt) at 30 bar hydrogen pressure and 290 °C (0.02 mol% Pt to BT) [12]. However, not only is full hydrogenation of the carrier relevant for the application of the LOHC technology, but depending on the amount of hydrogen that should be stored, partial loading of the carrier can be required. There-

[1]Barbara Bong https://orcid.org/0000-0003-4978-2480, Dr. Chalachew Mebrahtu https://orcid.org/0000-0001-6122-0937, Prof. Dr. Regina Palkovits https://orcid.org/0000-0002-4970-2957 (r.palkovits@fz-juelich.de)
Forschungszentrum Jülich GmbH, Institute for a Sustainable Hydrogen Economy, Marie-Curie-Straße 5, Jülich 52428, Germany.
[2]Barbara Bong, Dr. Chalachew Mebrahtu, Prof. Dr. Regina Palkovits Heterogeneous Catalysis and Technical Chemistry, Institute for Technical and Macromolecular Chemistry, RWTH Aachen University, Worringerweg 2, Aachen 52074, Germany.
[3]Dr. Wassja A. Kopp https://orcid.org/0000-0001-8147-3464, Thomas Nevolianis https://orcid.org/0000-0003-4478-5842, Prof. Dr. Kai Leonhard https://orcid.org/0000-0001-6231-6957
Institute of Technical Thermodynamics, RWTH Aachen University, Schinkelstraße 8, Aachen 52062, Germany.

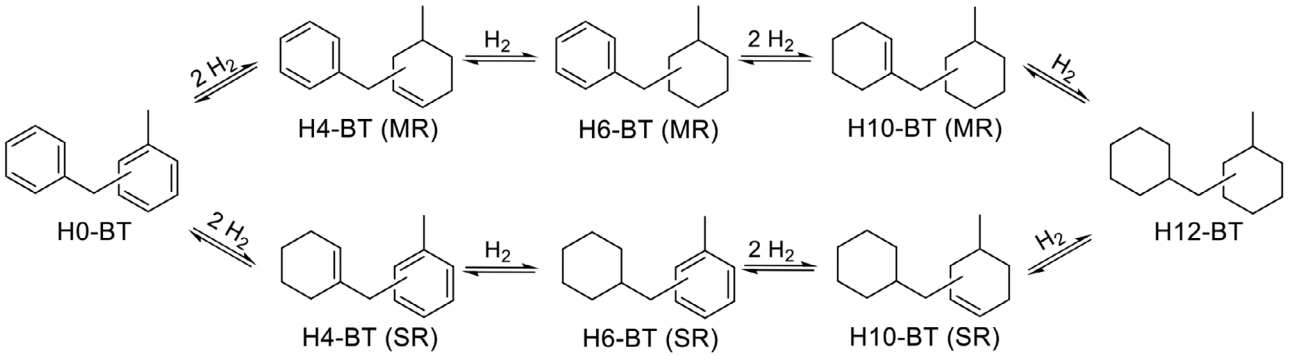

Scheme 1. Main reaction steps of the hydrogenation of benzyltoluene (H0-BT) to perhydro benzyltoluene (H12-BT) via preferred hydrogenation of the main ring (MR) or the side ring (SR) as reported in the literature [16, 26].

fore, besides the full hydrogenation of H0-BT to H12-BT, the intermediate steps play an important role [23–25]. The main reaction steps of the hydrogenation of benzyltoluene are shown in Scheme 1.

The main intermediate during the hydrogenation of H0-BT is H6-BT, where only one of the two aromatic rings has been hydrogenated. The hydrogenated ring can either be the toluene-ring (main ring [MR]) or the benzene-ring (side ring [SR]). Experimental studies showed that hydrogenation of the SR seems to be favored over the hydrogenation of the MR, but both reaction pathways can occur [12, 16, 17, 24, 27]. Besides H6-BT, small amounts of H4-BT and H10-BT intermediates are found in the hydrogenation reaction mixture, as experimental studies show [16, 17, 26]. These experimental findings are in accordance with expectations based on general thermodynamics, as the molecules H0-, H6-, and H12-BT with either a fully or not hydrogenated ring are supposed to have the lowest energy levels [12, 16, 26]. Species with only one hydrogenated double bond per ring (H2- or H8-BT) are expected to have the highest energy level and, thus, should occur in the lowest concentrations. H4- and H10-BT with two hydrogenated double bonds per ring should have a slightly higher share in the reaction mixture due to lower energy compared to H2- and H8-BT [16]. In this study, we therefore focus on H0-, H6-, and H12-BT as protagonists of BT-based hydrogen-carrying processes. Besides the non-, partially, or fully hydrogenated species, different isomers of each HX-BT species occur. As the starting material H0-BT is technically available as an isomeric mixture of *ortho*-, *meta*-, and *para*-benzyltoluene; respective isomers of the hydrogenated HX-BT species can occur in the reaction mixture [12, 13, 16, 26]. Experimental studies showed no noticeable isomerization during the hydrogenation reaction, meaning that the original ratio of the *ortho*, *meta*, and *para* isomers as well as their corresponding hydrogenated species is constant during the reaction [12, 16]. In addition to the substitution pattern (*ortho*/*meta*/*para*), further isomers of each species can occur due to the configuration of the substituents (*cis*/*trans*) and the conformation of cyclohexane (chair/boat). All in all, this results in three isomers for H0-BT, 18 for H6-BT, and 24 for H12-BT [12, 16, 26, 28]. Further conformational isomers may arise due to torsion around the single bonds linking MR and SR [28]. All of these isomers are considered in the calculations of this study.

To identify feasible conditions to load and unload HX-BT derivates, it is crucial to know the thermochemical properties of the participating isomers within the temperature and pressure range under study. In this way, the reaction steps and influences of the different isomers participating in the hydrogenation can be analyzed, and thus, the resulting information can be used for chemical engineering process models to further establish the application of hydrogen storage and transport by LOHC [12, 16, 26, 27]. Yet, for the LOHC system BT, chemical equilibrium compositions as limits of kinetic processes have so far not been computed. Only a few experimental and computational studies have reported some thermochemical properties of BT [14, 27]. (More thermodynamic data can be found for similar molecules like benzene [29, 30], diphenylmethane [29, 31, 32], methylbiphenyl [31], dibenzyltoluene [14, 24], and their respective hydrogenated species.) For H0- and H12-BT, Müller et al. [14] obtained thermochemical properties like heat capacity, enthalpy of formation, vapor pressure, and vaporization enthalpy. The thermochemical analysis performed by Verevkin et al. [27] includes different HX-BT species besides H0- and H12-BT, and they experimentally analyzed the thermochemical properties of each H0-BT isomer (*ortho*-, *meta*-, and *para*-BT) as well as an isomeric mixture of partially hydrogenated H6-BT and of fully hydrogenated H12-BT [27]. The different BT species were obtained by experimentally performing the hydrogenation of H0-BT, and afterward, isolation of the species by distillation steps. The extensive experimental effort in this study enabled the determination of the vapor pressure, enthalpies of vaporization, and enthalpies of formation for H0-, H6-, and H12-BT through combustion calorimetry [27]. These experimental results were corroborated by quantum chemical G3MP2 calculations. To obtain the most stable conformation, a force-field-based study using MMFF94 was performed. This was conducted for each H6- and H12-BT isomer. Then, the composite G3MP2 method was used to obtain enthalpies of formation and Gibbs free energies using the rigid-rotor harmonic oscillator (RRHO) model. Furthermore, the enthalpy of reaction varied depending on the reaction step and the specific isomer and specific ring taking part in the reaction. Even though the effects are weak, they were observable [27]. This emphasizes that thermodynamic data of all different HX-BT species should be considered to study the overall hydrogenation reaction [27]. From the RRHO Gibbs free energies, gas-phase molar fractions of different substitutions for each isomer were calculated; e.g., molar fractions of the six isomers of H6-BT formed by hydrogenation of the SR or MR at *ortho*, *meta*,

or *para* positions were calculated. To analyze the conformational mixture within floppy molecules like BT derivates, an RRHO treatment is no longer considered today as state-of-the-art to obtain reliable entropies and thereby Gibbs free energies [33, 34].

This study aims to compute reliable temperature- and pressure-dependent chemical equilibrium compositions and, hence, considers all possible isomers for the important HX-BT species H0-, H6-, and H12-BT. For the calculations, intermediates with partially hydrogenated rings like H2- or H4-BT are neglected as they are expected to be thermodynamically unfavored and were also not dominant in experimental studies. Entropies and thereby reaction equilibria can be strongly affected by internal rotations of heavy groups around single bonds. BT provides two such rotations within the two single bonds between the MR and SR (the internal rotation of the methyl group is present in reactants and products and is not expected to influence reaction equilibria). An RRHO treatment of molecular torsions can lead to errors in entropies of about 2 J mol^{-1} K^{-1} per rotation [33]. For larger alkanes, RRHO entropies were found to deviate more than 5 % from measurements. A state-of-the-art method to model the thermochemistry of molecular torsions is the one-dimensional (1-D) hindered rotor model. For larger alkanes, it yields entropies that deviate less than 1 % from measurements [35]. Therefore, in this study, a 1-D hindered rotor treatment of both torsions is used, thereby covering the various conformations present for each isomer. This leads to more accurate Gibbs free energies than RRHO, and these are provided over the whole temperature range of interest for the application of the BT-based LOHC system (25–280 °C). From that, we deduce equilibrium compositions for the gas and liquid phases.

The equilibrium composition received from the thermodynamic calculations is compared to the composition obtained from experimental investigations. For this purpose, the hydrogenation of H0-BT was performed at different reaction temperatures and for different reaction times. After the experiment was finished, the composition of the liquid phase was analyzed, giving the amount of each non-, partly, or fully hydrogenated species HX-BT. The experimentally obtained composition is compared to the calculated equilibrium composition. In this way, further insights into the influences on the hydrogenation of H0-BT are gained, which can be applied to identify feasible conditions for the loading and unloading of the H0-BT/H12-BT LOHC systems.

2 Experimental Methods

2.1 Safety Warning

High-pressure experiments using hydrogen must be conducted only under rigorous safety precautions with appropriate equipment.

2.2 Materials

Benzyltoluene (H0-BT) was supplied as an isomeric mixture of *ortho*-, *meta*-, and *para*-H0-BT (trade name: Marlotherm LH) by Eastman Chemical Company. Titania pellets (anatase) were purchased from abcr GmbH. $Pt(NH_3)_4(NO_3)_2$ (≥50.0 % Pt basis) and tetradecane (purity ≥99.0 %) were obtained from Sigma Aldrich. Dichloromethane (purity ≥99.9 %) was sourced from Honeywell. No further purification of the chemicals was performed.

2.3 Catalyst Synthesis and Characterization

The Pt/TiO_2 catalyst (0.3 wt% Pt) was synthesized via a wet impregnation method following the procedure by Chen et al. [36]. The desired platinum loading of the prepared catalyst was confirmed by inductively coupled plasma optical emission spectroscopy. Further information on the catalyst preparation as well as its characterization is provided in the Supporting Information (SI; Preparation of the Pt/TiO_2 Catalyst).

2.4 Hydrogenation Experiments

Hydrogenation experiments with a reaction time of up to 10 h were performed in stainless-steel pressure reactor (Parr Micro Benchtop reactor 4590, 50 mL) coupled to a gas burette. The experimental procedure for these experiments was adapted from a previous publication by some of us [37]. H0-BT as well as the catalyst powder (platinum to substrate ratio of 0.2 mol %) were inserted into the reactor. Then, the reactor system was closed and flushed with hydrogen three times. Next, the hydrogen pressure in the reactor was adjusted to the desired value via a pressure regulator. The gas burette was pressurized with approximately 100 bar hydrogen pressure. Afterward, the needle valve from the gas burette to the reactor was closed while the reactor was heated up to the desired reaction temperature under stirring. During the reaction, the needle valve can be opened to keep the pressure inside the reactor constant by feeding hydrogen from the burette into the reactor.

Long-term experiments (>12 h reaction time) were performed in a stainless-steel batch autoclave (50 mL) equipped with a stirring bar. H0-BT and the catalyst powder were added into the autoclave; the system was closed and flushed with hydrogen three times. Afterward, the autoclave was pressurized with hydrogen at the desired reaction pressure and placed in a pre-heated heating mantle.

For all hydrogenation experiments, the start of the reaction was defined at the time when the reaction temperature was reached. After each reaction, the reaction vessel was cooled down. Then, the stirring was stopped, and the system was depressurized. The reaction mixture was taken out, and the catalyst was separated from the liquid phase by filtration.

2.5 Liquid-Phase Analysis

The composition of the reaction liquid was analyzed by gas chromatography and mass spectrometry as reported in a previous publication by some of us [37]. Using this analysis method, the amount of each HX-BT in the reaction mixture was quantified.

To quantify the overall hydrogen loading of the carrier compound, the degree of hydrogenation (DOH) can be utilized. The DOH of the liquid phase was calculated from the molar fraction

x of each species HX-BT with X hydrogen as commonly used in literature (Eq. 1) [17, 36, 37]:

$$\mathrm{DOH_{BT}} = \sum X\ 12^{-1} x\,(\mathrm{HX\text{-}BT}) \tag{1}$$

3 Computational Methods

3.1 Calculations

Harmonic vibrational frequencies have been calculated for optimized geometries. Geometry optimizations have been performed using the B3LYP density functional [38–41] and Grimme's D3 dispersion correction with Becke–Johnson damping [42]. A very fine integration grid (199 radial and 974 angular points per atom) was used together with very tight SCF convergence criteria. We used Ahlrichs triple-zeta valence polarizable basis set tzvp [43, 44]. The same B3LYPD3BJ/tzvp level of theory was used for the frequency calculations; B3LYP is known to be efficient and performs very well for vibrational frequencies [45]. The frequencies have been used unscaled for the determination of thermochemical data from RRHO partition functions, as detailed investigations of B3LYP bias in frequency computations revealed that scaling factors for thermochemical data approximately amount to unity [46].

The two rings in BT are linked by two single bonds around which the molecule exhibits torsional motion. This torsion is not a free rotation but is influenced by the potential energy as a function of the torsional angle. We performed potential energy scans along each of these two torsional angles to determine this function. If a lower energy minimum was found during these rotations, we repeated all optimizations, frequency calculations, and scans based on that lowest energy minimum. Though calculations therefore refer to the lowest energy conformation, higher conformations show up within the potential energy profiles of the scans. The scans were performed in 30 steps of 12° and, in case the scan did not end in the initial structure, also in −12° steps. All geometry optimizations and frequency calculations were done using the Gaussian software version 16 c01 [47].

From the harmonic vibrational frequency calculations and the torsional scans, we computed thermochemical data within a hindered rotor model using TAMkin [48] and our TAMkinTools extension [49]. We fitted a Fourier series of order 50 to each torsional energy profile. Within TAMkinTools, in addition to minimizing the deviation from the computed potential energy points, the curvature along a grid is also minimized. This avoids a frequent issue with oscillations in scans with steep and flat regions and allows the use of Fourier series of high orders. For each hindered rotation, the corresponding 1-D Schrödinger equation is solved using a Fourier-type basis set with 1000 elements. This leads to 1000 energy levels as solutions to the Schrödinger equation, a high number that is needed to obtain converged thermochemical data at higher temperatures. To combine the hindered rotors with the RRHO partition function, TAMkin fits a parabola to the potential energy shape in the minimum and creates an extra HO partition function. Then, the total RRHO partition function is divided by that extra function and multiplied by the corresponding HR partition function.

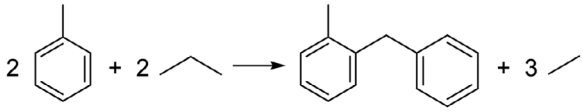

Scheme 2. Reaction scheme for the formation of benzyltoluene from toluene and propane.

The energies of all structures have been corrected by single-point-coupled cluster calculations with the delocalized pair natural orbital (DLPNO) approximation. The energies were extrapolated to the basis set limit based on two calculations with finite cc-pvtz and cc-pvqz calculations [50, 51]. DLPNO-approximated energies are known to deviate from non-approximated CCSD(T) energies far less than 1 kcal $\mathrm{mol^{-1}}$ [52]. These calculations were done using ORCA 5 [53].

Enthalpies of formation, heat capacities, and entropies were obtained from the partition functions computed by TAMkin. Standard heats of formation need to be computed with respect to a meaningful reference. Compound methods in computational chemistry are often trained on atomization data. In turn, using reference reactions that keep most groups in the molecules unchanged (i.e., isodesmic reactions) benefits from systematic error cancellation of the ab initio calculations involved. Here, we computed the standard heat of formation of benzyltoluene from the reaction of toluene and propane as shown in Scheme 2.

The required experimental data were found in the NIST database [54] as −84 kJ $\mathrm{mol^{-1}}$ for ethane [55], −104.7 kJ $\mathrm{mol^{-1}}$ for propane [56], and 50.1 kJ $\mathrm{mol^{-1}}$ for toluene [57].

We computed free energies of solvation using the COSMO-RS model [58–60]. Ensemble solution-phase geometries of the species were optimized using COSMOconf [61] at BP-TZVP-COSMO level of theory. Once the solution-phase geometries are obtained, the free energies of solvation are calculated with COSMOtherm [62], where a pure ideal gas with a concentration of 1 mol $\mathrm{L^{-1}}$ and the solute dissolved at infinite dilution with a reference concentration of 1 mol $\mathrm{L^{-1}}$ is used as the reference state. More details regarding the selection of the reference state can be found in the recent study by some of the authors [63] as well as in the SI. Because gas-phase calculations showed H0-BT and H12-BT to be the dominant species, we computed Gibbs free energies of solvation referring to binary mixtures of H0- and H12-BT in molar fraction steps of $\Delta x = 0.2$. For the liquid phase, we chose the isomers with lowest free energy in the gas phase as representatives for each of H0-, H6-, and H12-BT. The actual isomer mix will depend both on the initial sample and on the applied catalyst. Gibbs free energies of solvation at standard temperature vary by less than 1 kcal $\mathrm{mol^{-1}}$ with mixture composition, cf., SI. The following temperature-dependent analysis therefore uses Gibbs free energies of solvation evaluated only in both limits, i.e., in 100 % H0-BT or 100 % H12-BT.

The four molar fractions that are assumed to make up the total liquid-phase composition, i.e., the fractions of H_2, H0-BT, H6-BT, and H12-BT, can be determined from four equations. The molar fraction of physically absorbed H_2 in the liquid phase x_{H_2} is then computed from Henry's law:

$$x_{\mathrm{H_2}} = \frac{p}{H\,(T)}\, x_{\mathrm{gas,H_2}} \tag{2}$$

$$\text{H0-BT} + 3\,\text{H}_2 \overset{K_1}{\rightleftharpoons} \text{H6-BT}$$
$$\text{H6-BT} + 3\,\text{H}_2 \overset{K_2}{\rightleftharpoons} \text{H12-BT}$$

Scheme 3. Simplified hydrogenation reaction scheme.

For lower temperatures and higher pressures, the molar fraction of H_2 in the gas phase x_{gas,H_2} can be assumed to amount to unity. In general, the vapor–liquid equilibrium needs to be considered explicitly, in which the total pressure equals the sum of LOHC components' vapor pressures times their mole fraction and Henry constant of H_2 multiplied by its mole fraction in the liquid phase. This general treatment that couples reaction equilibria in gas and liquid phases to vapor–liquid equilibrium is implemented in our current model (cf., repository https://doi.org/10.5281/zenodo.14143841) and holds for thermochemical equilibrium below the boiling point. The equations comprise the gas- and liquid-phase concentrations of H_2, H0-BT, H6-BT, and H12-BT of representative isomers. The influence of further isomers is expected to be small and neglected for thermochemical equilibrium computation. Concentrations of other partly hydrogenated species, like, e.g., H4-BT have been found to be small and are neglected as well. The equilibrium could be disturbed if components are rapidly entered into or removed from one of the phases. To treat hydrogenation computationally, we simplify the reaction scheme from Scheme 1 in a two-step process as displayed in Scheme 3.

This determines the remaining three molar fractions: two follow from the law of mass action for the two reaction equations of Scheme 3, and the last from the closure condition.

The molar fraction of H6-BT reads $x_{\text{H6-BT}} = x_{\text{H0-BT}} x_{\text{H}_2}^3 K_1(T, \{x\})$ using the molar fraction $x_{\text{H0-BT}}$ of H0-BT and the molar fraction of H_2 from Eq. (2).

The equilibrium constant of the first reaction in Scheme 3 (K_1) is calculated for an explicit liquid-phase composition $\{x\}$. The molar fraction of H12-BT follows analogously from $x_{\text{H12-BT}} = x_{\text{H6-BT}} x_{\text{H}_2}^3 K_2(T, \{x\}) = x_{\text{H0-BT}} x_{H_2}^6 K_1(T, \{x\}) K_2(T, \{x\})$. The equilibrium constant K_2 refers to the second reaction of Scheme 3. These equations, together with the closure condition $\Sigma x_i = 1$ allow to compute the complete composition of the liquid phase. With the assumption of a gas phase of approximately 100 % H_2, the compositions can be computed analytically. In this study, we solve for the partial pressures following from reaction and vapor–liquid equilibria. This requires iterative solution, which we have implemented in a sheet on the repository (see https://doi.org/10.5281/zenodo.14143841). There, we provide the compositions, i.e., molar fractions of H_2, H0-BT, H6-BT, and H12-BT.

4 Results and Discussion

4.1 Gas-Phase Thermodynamics of Benzyltoluene-Based Isomers

Free energies, entropies, and enthalpies have been computed for all isomers for the ideal gas state first (cf., tables in SI). For the non-hydrogenated H0-BT form, there are just the three *ortho*, *meta*, and *para* isomers. The *ortho* form is 1.5–2 kJ mol^{-1} lower in energy than *meta* and *para*, but also lower in entropy by about 25 J mol^{-1} K^{-1}. The actual isomer mix in thermochemical equilibrium is determined by the energy–entropy interplay and resulting Gibbs free energies for *ortho* are higher by 6.8–10.8 kJ mol^{-1}. H0-BT structures are computed to be about 12 kJ mol^{-1} higher in energy than the G3MP2-based computational results by Verevkin et al. [27] but in good agreement with their correction obtained from a correlation to experimental data of similar compounds. This indicates that the overall computational approach of this study yields accurate enthalpies, entropies, and Gibbs free energies.

The partly hydrogenated H6-BT shows 18 isomers in total. When the SR is hydrogenated, it can be in boat or chair configuration. When the MR is hydrogenated, the methyl group can be in *cis* or *trans* position. This yields $3 \times (2 + 2 \times 2)$ possible isomers. Throughout, the boat isomers show energies higher by 20–30 kJ mol^{-1} than the chair isomers, with entropies being similar. One can thus neglect boat isomers for most applications. Energies for *cis* and *trans* isomers for the hydrogenated MR vary in a range of 7 kJ mol^{-1} without a clear trend; one of the two is always close in energy and entropy to the corresponding SR isomer. Verevkin et al. [27] report energies in close agreement with our calculations, while accounting only for the dominant chair (and *cis*) isomers (the lowest energy isomers are partly *trans*, though, and not *cis* as used by Verevkin et al. [27]). The lowest energy structure emerging from our calculations, i.e., *para*-chair (SR), is 6 kJ mol^{-1} lower than the experimental result of −76 kJ mol^{-1}. Entropies vary around 491 ± 5 J mol^{-1} K^{-1} with two outliers: H6-BT *meta*-boat/chair (516/510 J mol^{-1} K^{-1}). These outliers are due to the low frequencies (<100 cm^{-1}) being 10–20 cm^{-1} lower than for the other isomers from this study. This makes the *meta*-chair structure dominate Gibbs free energy and population. In the H6-BT reaction mixtures by Verevkin et al. [27], the *para* and *ortho* SR were predominantly found as reaction products, which indicates that this mixture is not produced in chemical equilibrium. Instead, the same isomers as in the H0-BT mixture are dominant, probably because the isomer type is conserved during the reaction. In chemical equilibrium below 250 °C, H6-BT is preferred over H0-BT + 3H_2.

The fully hydrogenated H12-BT species appears in 24 isomers because of the two orientations of the methyl group and both chair/boat conformations of the main and side rings. The isomers differ largely in energy, the lowest being all-chair *para–trans* (−291 kJ mol^{-1}) and all-chair *meta–cis* (−289 kJ mol^{-1}). These structures are more than 12 kJ mol^{-1} lower than the lowest energy species reported by Verevkin et al. [27] and 16 kJ mol^{-1} lower than the experimental results. Entropies vary around 505 ± 6 J mol^{-1} K^{-1} without large outliers. Consequently, these two isomers dominate Gibbs free energies at standard temperature. Because their Gibbs free energies are also considerably lower than Gibbs free energies for H6-BT + 3H_2 and H0-BT + 6H_2, the fully hydrogenated species dominate chemical equilibrium over wide ranges of temperature and pressure. Entropies for H12-BT are much lower than entropies for H6-BT + 3H_2 and H0-BT + 6H_2, so that the corresponding Gibbs free energies for H12-BT increase much stronger with temperature than those of H6-BT and H0-BT. Around 225 °C, H12-BT species are overtaken by H6-BT, which dominate the equilibrium

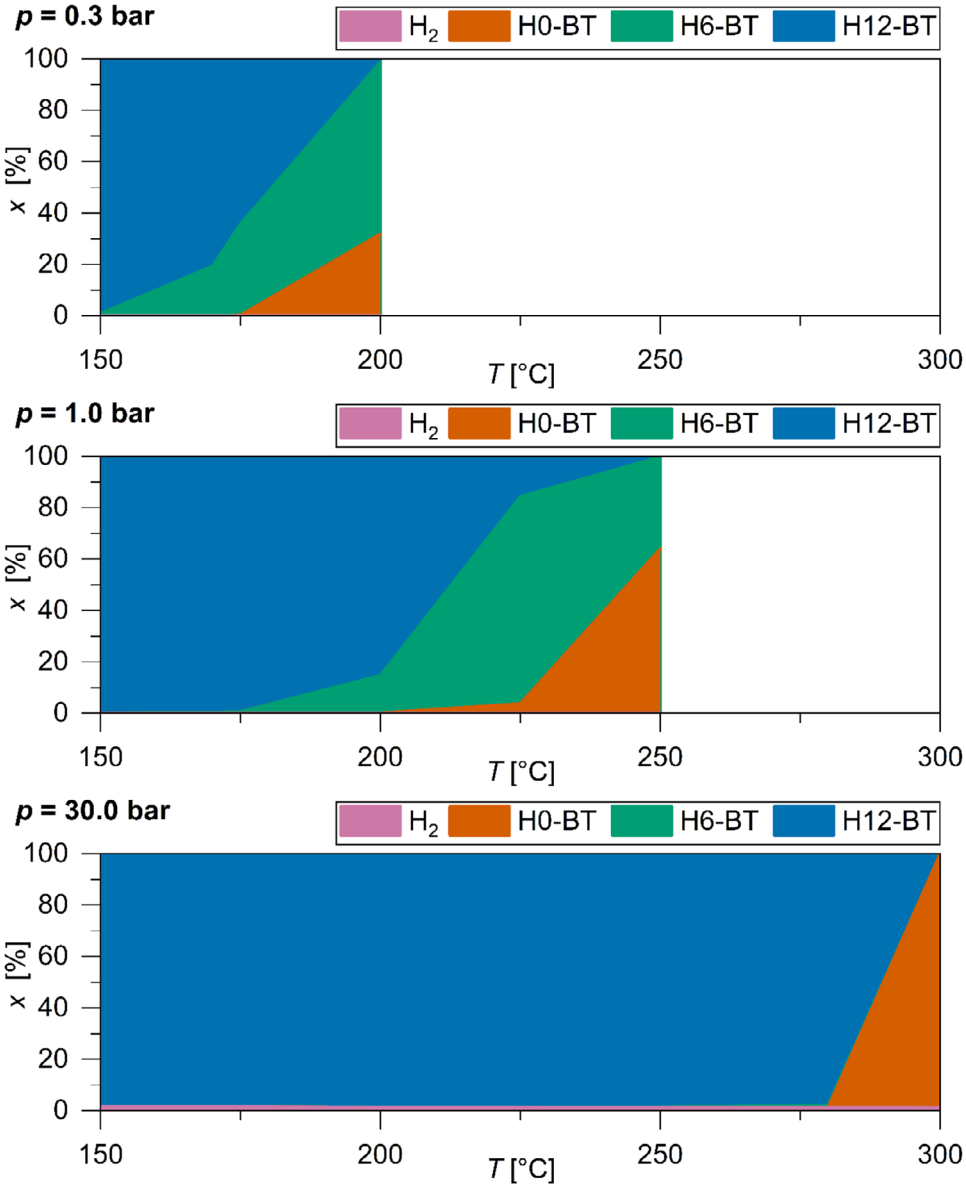

Figure 1. Calculated liquid-phase composition in chemical equilibrium at pressures of 0.3, 1.0, and 30.0 bar; the amount of H_2 is less than 2 % for all shown conditions; data are provided in the repository (https://doi.org/10.5281/zenodo.14143841).

composition at high temperature. In their H12-BT reaction mixture, Verevkin et al. [27] find predominantly *para* and *ortho* H12-BT, which is probably affected by the reaction procedure and not in complete chemical equilibrium, similar to the H6-BT mixture.

4.2 Liquid-Phase Reaction Equilibria

H_2 from the gas phase is absorbed to a low extent in the LOHC liquid phase, weakly dependent on temperature and strongly dependent on pressure as well as the partial pressure of evaporated LOHC. In order to model reaction equilibria in liquid phase, we performed COSMO-RS calculations, as described in Section 3, for the dominant species determined in the preceding gas-phase analysis. Henry constants for H_2 vary from 1750 bar at 25 °C to 2650 bar at 280 °C in H0-BT and from 1500 to 2500 bar in H12-BT. This leads to H_2 concentrations in the order of 2 % at high pressure (30 bar) down to far below 0.1 % at 1 bar.

Chemical equilibrium compositions limit the kinetic loading and unloading processes and follow, using the law of mass action, from the temperature-dependent Gibbs free energies in gas and liquid phases. Gibbs free energies of solvation are quite similar for all three considered hydrogenation stages of HX-BT species (H0-, H6-, and H12-BT) and mostly differ at low temperature and in H0-BT. In H12-BT solvent, differences between BT derivates are less than 4 kJ mol^{-1} at all temperatures. Therefore, the mixture composition at chemical equilibrium in the liquid phase closely resembles the gas-phase composition. Yet, this is the first study presenting BT compositions, i.e., fractions of absorbed H_2 as well as H0-, H6- and H12-BT, at wide temperature and pressure ranges, cf., Fig. 1.

The main characteristics of BT loading and unloading can be inferred from these chemical equilibrium data in Fig. 1. At "low" temperature, dependent on pressure up to 150 or 270 °C, the equilibrium is heavily on the H12-BT side; practically the mixture purely consists of H12-BT and a small amount of hydrogen. At most pressures, there is a range of 30–60 K where substantial amounts of H6-BT can be present. At high temperatures, the non-hydrogenated species H0-BT is favored. Accordingly, based on equilibrium compositions, loading and unloading of BT-based LOHC depends in practice more on pressure than on temperature. Pressures below 1 bar can be relevant to account for dilution by further gases, e.g., air for combustion of released H_2. For stoichiometric combustion, the partial pressure of H_2 corresponds to 0.3 bar. Neglecting the absorption of spurious amounts of these further gases in the liquid phase, the model equations become equivalent to setting the total pressure to 0.3 bar, cf., SI. Although such a reduced pressure of 0.3 bar leads to partial dehydrogenation at around 175 °C, at high pressure of, e.g., 30 bar, the mixture in chemical equilibrium stays fully hydrogenated up to 280 °C. Hence, high temperature reduces the amount of partly hydrogenated species.

4.3 Experimental Study of the Reaction Mixture Obtained by Hydrogenation of Benzyltoluene

The results obtained from the thermochemistry calculations and experimental studies of the hydrogen loading of H0-BT are collated. For this purpose, the hydrogenation of H0-BT was performed using an established platinum on oxide catalyst (Pt/TiO_2, 0.2 mol% Pt to H0-BT, batch process) with BT in liquid state (further information on the experimental procedure is provided in the SI). To obtain further insights into the thermochemistry of the reaction, the composition of the reaction mixture obtained for experimental hydrogenation runs with different reaction times and temperatures is compared to the results from thermodynamic calculations.

To study the temperature influence on the hydrogenation process, the DOH values obtained after 1 h of reaction time at a constant hydrogen pressure of 30 bar are evaluated for reaction temperatures between 125 °C and 225 °C (Fig. 2).

The hydrogen loading of H0-BT was favored at all reaction temperatures between 125 and 225 °C employed in this study. However, the DOH obtained after 1 h of reaction time increases strongly with increasing reaction temperature. While the hydrogenation at 225 °C led to full loading of H0-BT (DOH = 1.00), a mean DOH of 0.84 ± 0.12 was reached at 200 °C (further information on the deviation between the results obtained by the different experimental runs is given in the SI, Deviation of Experimental Results of Hydrogenation). Hydrogenation at 125 °C resulted in a DOH of 0.15 after 1 h. These results obtained at different reaction temperatures indicate that the overall reaction rate is strongly influenced by the temperature. Therefore, limitation of these reactions by kinetic factors instead of the thermodynamic equilibrium can occur, especially if the kinetic is slowed down by a decrease in the reaction temperature. Thus, the thermodynamic equilibrium is probably not reached after 1 h of reaction time under the employed reaction conditions. The detailed course of the reaction at 125 °C is visualized in Fig. 3. To

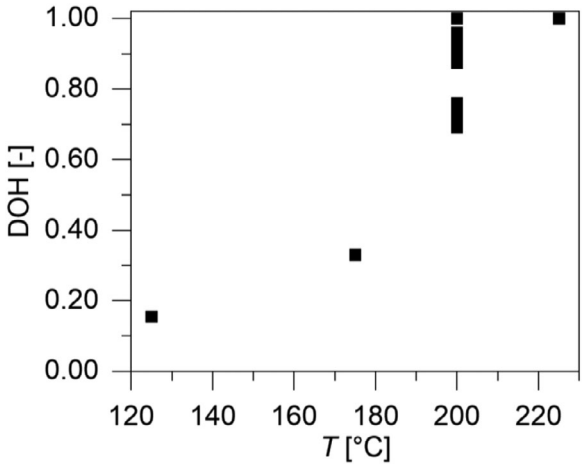

Figure 2. Temperature influence on the hydrogenation of H0-BT using Pt/TiO_2 catalyst (0.02 mol% Pt to H0-BT), constant hydrogen pressure of 30 bar, and 1 h of reaction time.

gain further insights into the reaction route, not only the overall DOH is considered, but also the composition of the reaction liquid consisting of the different HX-BT species for representative samples obtained after different reaction times is given. After 30 min of reaction time, the main compound in the reaction mixture was still the substrate H0-BT (93.6 %), but also the partially hydrogenated H6-BT was present (6.0 %). Furthermore, a small amount (0.3 %) of the fully hydrogenated H12-BT has been formed. Additionally, 0.1 % of H4-BT was detected. This composition of the reaction mixture refers to an overall DOH of 0.07. For longer reaction times, the DOH increased with the consumption of H0-BT and the formation of H6- and H12-BT. After 480 min, the reaction mixture consisted mainly of H12-BT (93.2 %). Over the course of the reaction, the HX-BT species with two hydrogenated double bonds per ring (H4- or H10-BT) were found, but the ratio of these compounds was at any point less than 1 %. H2-BT and H8-BT were not detected. These results are in accordance with the expectation that the energy level decreases from the HX-BT species with only one hydrogenated double bond per ring (H2- or H8-BT) over species with two hydrogenated double bonds per ring (H4- or H10-BT) to molecules with either a not or fully hydrogenated ring (H0-, H6-, or H12-BT) [12, 16, 26]. Hence, the ratio of each species in the reaction liquid increases with the decreasing energy level. Even though trace amounts of H4- and H10-BT were detected in the reaction mixture, they can be neglected due to their low concentrations. The obtained course of H6-BT and H12-BT over the reaction time suggests a consecutive reaction path in the hydrogenation of H0-BT to H12-BT.

The comparison of these experimental results to the calculated equilibrium composition gives further insights into the hydrogenation process. According to the calculated composition, only H12-BT was still present in the equilibrium at 30 bar hydrogen pressure and 125 °C (see Fig. 3). For the experimental hydrogenation at 125 °C and 30 bar hydrogen pressure, the reaction liquid obtained after 480 min consisted mainly of H12-BT (93.2 %) but 6.7 % of H6-BT was still present. For the experimental hydrogenation at 225 °C, only H12-BT was detected in the

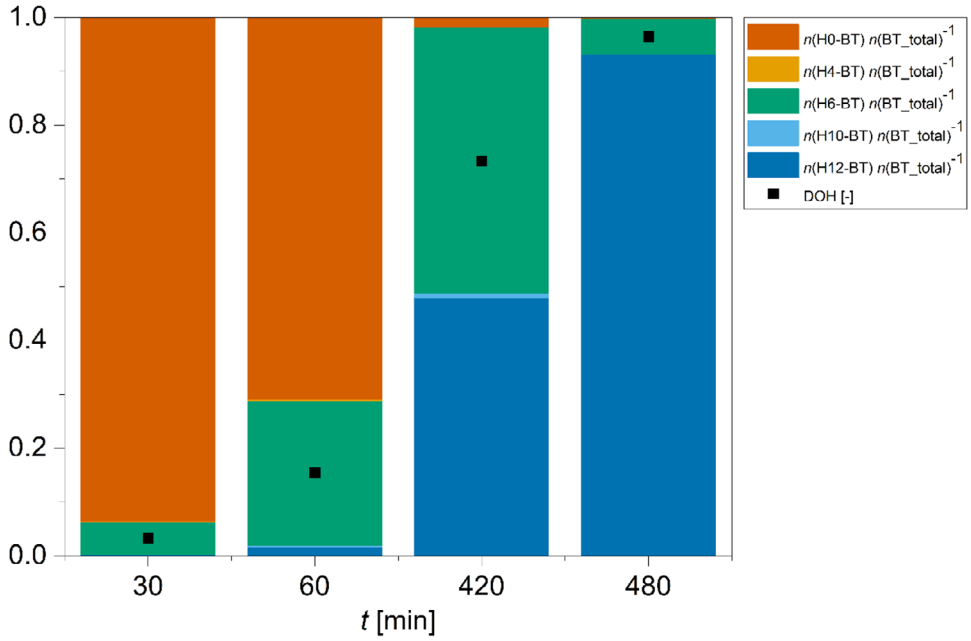

Figure 3. Course of the hydrogenation of H0-BT at 125 °C using Pt/TiO_2 catalyst (0.02 mol% Pt to H0-BT) and constant hydrogen pressure of 30 bar.

reaction liquid after 60 min. According to the calculations, the amount of H6-BT increases slightly with increasing temperature, but only about 1 % of H6-BT is formed at a high temperature of 280 °C (see Fig. 3). Thus, the experimentally obtained data for the reaction at 225 °C are in accordance with the calculated composition. The increase of the reaction temperature from 125 to 225 °C at 30 bar hydrogen pressure does not significantly change the equilibrium composition (see Fig. 1), but at lower temperatures the reaction proceeds slower than at higher temperatures. Therefore, the thermodynamic equilibrium was probably not reached after 480 min at a reaction temperature of 125 °C. These results indicate a significant contribution of the kinetics on the hydrogenation reaction under the employed reaction conditions.

To experimentally analyze the composition of the reaction liquid close to or at equilibrium, the reaction conditions must be adjusted so that the thermodynamic equilibrium could be reached under the given conditions. For the real reaction approaching equilibrium, limitations can occur, which could impede reaching equilibrium [64]. Nevertheless, the obtained reaction liquid close to equilibrium can be compared to the calculated equilibrium composition. For this purpose, a long-term hydrogenation reaction (2 weeks reaction time) was performed at 200 °C. In this case, the reaction vessel was pressurized at 30 bar hydrogen pressure in the beginning, and the pressure decreased as hydrogen was consumed during the ongoing hydrogenation. The measured hydrogen pressure stabilized at nearly 0 bar, meaning that no detectable amount of hydrogen was left in the gas phase of the reaction. In this experiment, a DOH of 0.211 was obtained. The composition of the liquid phase obtained after this long-term experiment is compared to the theoretical equilibrium composition (Fig. 4). For this purpose, the equilibrium composition at 200 °C regarding the DOH of 0.211 was calculated, resulting in a calculated pressure of 0.24 bar (cf., SI). For the Gibbs free energy of solvation calculations, here the H0-BT reference limit was used, given that H0-BT is the dominant species.

The experimentally obtained reaction liquid consisted mainly of H0-BT (60.4 %) and H6-BT (37.0 %). These amounts agree with the calculated amounts of 58.1 % H0-BT and 41.7 % H6-BT. As H4- and H10-BT were not detected in the reaction liquid, the expectation that these species occur in the lowest concentrations is confirmed. Furthermore, the assumption that only H0-, H6-, and H12-BT needed to be considered in the calculation is validated. In the calculated composition, only an imperceptible amount of H12-BT is present (0.3 %), but the reaction liquid contained a significant amount of H12-BT (2.5 %). This small deviation between experimental and calculated amounts indicates that the formation of H12-BT is favored under real experimental conditions. Possibly, under the given conditions, the dehydrogenation of H12-BT was hindered, or the hydrogenation of H6- to H12-BT proceeded faster than the backward reaction of forming H6-BT via the dehydrogenation of H12-BT. In this case, the equilibrium between H6- and H12-BT would not have been achieved in the experiment, resulting in a higher amount of H12-BT in the reaction liquid than in the equilibrium composition. Furthermore, a small deviation between the experimentally obtained and the theoretical composition can also be caused by the assumptions employed during the calculations. All in all, the presented results show that the experimental and theoretical data are in good agreement, and in general, the calculated equilibrium compositions can reflect the real composition.

Under real reaction conditions, the limiting factors are probably not thermodynamic effects but kinetic aspects. Thus, to reach the thermochemical equilibrium, the respective conditions must be adjusted, e.g., an increase in reaction temperature can be used to increase the reaction rate, as shown in the experimental

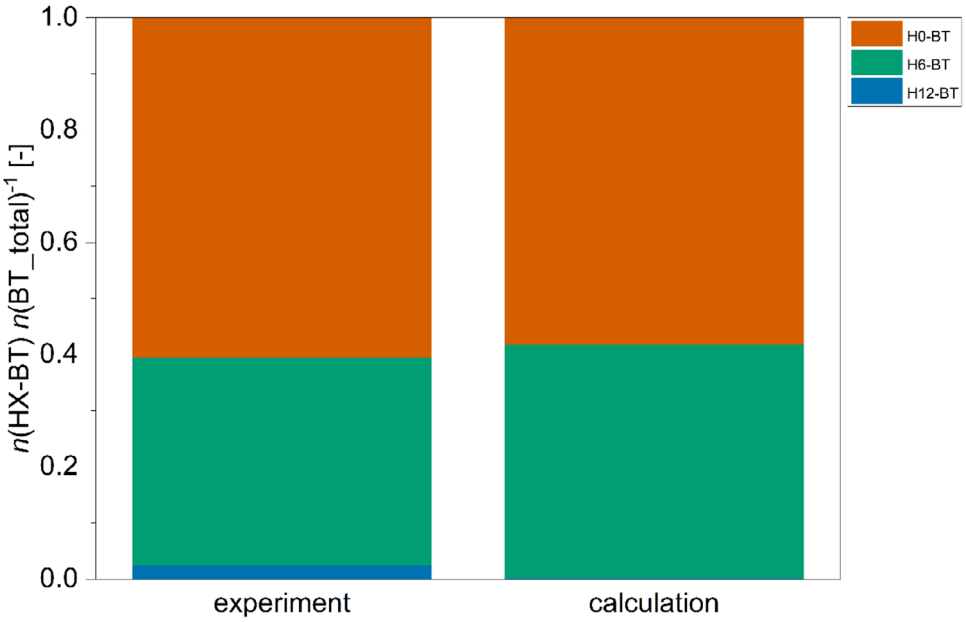

Figure 4. Composition of the liquid phase obtained in the long-term hydrogenation experiment (2 weeks reaction time, 200 °C, 30 bar initial hydrogen pressure) and the calculated composition at similar parameters (200 °C, DOH = 0.211); the calculated amount of H12-BT is less than 1 % and, thus, hardly visible.

study of the temperature influence. As shown from the results of the thermodynamic calculations and validated by analysis of the experimentally obtained reaction liquid, the equilibrium composition obtained in the hydrogenation/dehydrogenation reaction can be influenced by the chosen pressure and temperature.

Although hydrogenation is an exothermic reaction and therefore generally less favorable at higher reaction temperatures, the calculations from this study underline the crucial role of (hydrogen gas) pressure. At conditions of 30 bar, the chemical equilibrium favors hydrogenation at almost all temperatures up to the boiling temperature of the LOHC. Using the catalyst from this study, the equilibrium can be reached above 200 °C within 1 h of reaction time. For dehydrogenation, pressure needs to be lowered considerably; at 1 bar, dehydrogenation to significant amounts of H0-BT is thermodynamically possible only above 230 °C. Partial dehydrogenation (i.e., H6-BT formation from H12-BT) and thus, hydrogen release occurs already at temperatures lower by 50–75 K than full unloading of the LOHC (i.e., H0-BT formation). Based on these results, the technical application of the LOHC process can be optimized. First, pressure is decisive for the loading as well as the unloading. By pressure adjustment, the hydrogenation and dehydrogenation process can be performed at lower temperatures. Second, the consideration of partly loaded conditions is crucial for real applications where the amount of hydrogen to be stored does not always match with the amount of hydrogen for full hydrogenation. Analogously, during the hydrogen release, the amount of required hydrogen can correspond to partial dehydrogenation. Moreover, depending on the technical process, it can be attractive to operate the LOHC system mostly within partly loaded or unloaded conditions to opt for moderate temperature conditions. The requirement of high temperatures is currently a major drawback of the LOHC technology [15, 19]. Especially, reduction of the operation temperature and hence, reduction of the energy demand for heating, can increase the efficiency of the overall process. As shown by life cycle assessments for the similar LOHC systems dibenzyl toluene or toluene, heating of the dehydrogenation unit by burning natural gas or even hydrogen significantly increases the greenhouse gas emissions of the process [65, 66]. Therefore, temperature reduction by using low pressures together with suitable catalysts and by allowing for partly loaded conditions can be a game changer in hydrogen storage and transport for a sustainable hydrogen economy.

5 Conclusions

In this study, we have investigated partial and full hydrogen loading and unloading of the LOHC system benzyltoluene (H0-BT)/perhydro benzyltoluene (H12-BT). We have studied experimentally obtained hydrogenation kinetics for the hydrogenation of H0-BT using Pt/TiO_2 catalyst for various reaction times and temperatures. Chemical equilibrium compositions as limiting asymptotes of the kinetic measurements have been computed from ab initio and statistical mechanics methods. For the isomers of H0-, H6-, and H12-BT, thermochemical data have been computed, and the *meta* and *para* chair isomers were proven to be the most stable at all temperatures studied herein. For molecular geometries from DFT optimizations, energies were computed from DLPNO-accelerated and extrapolated coupled cluster theory. The two single bonds linking the MR and SR of HX-BT showed various conformations, which have been included within a hindered rotor treatment. This provided reliable enthalpies and entropies over a wide temperature range. Liquid phase data, including absorption of H_2, were calculated from the COSMO-RS model. From the law of mass action for the (de-)hydrogenation reactions, we computed equilibrium compositions as functions of temperature and pressure. BT-based hydrogenation and dehydrogenation equilibria were shown to be largely influenced by pressure. At loading conditions of 30 bar, chemical equilibrium favored complete hydrogenation

at all temperatures under study. Under vacuum at around 200 °C, dehydrogenation gets favored, increasingly at higher temperatures.

The experimental results for the hydrogenation of H0-BT demonstrated that the reaction proceeds via the partially hydrogenated species H4-, H6-, and H10-BT to H12-BT. The intermediate H6-BT occurred in relevant amounts, whereas H4- and H10-BT could be neglected. Under the equipped reaction conditions of 30 bar hydrogen pressure and temperatures up to 200 °C, the calculated equilibrium composition has not been reached, indicating kinetic control of the reaction. Up to this temperature, the equilibrium composition is largely temperature-independent and consists practically only of fully loaded H12-BT. In turn, in a long-term experiment in a closed vessel where pressure dropped due to H_2 being consumed by hydrogenation, substantial amounts of H0- and H6-BT were obtained, which is in accordance with the calculated amounts of these species in the equilibrium composition for low pressure.

The kinetic measurements showed how an increase in temperature allows to approach equilibrium conditions much faster. For the technical application of hydrogen loading of H0-BT, temperature can be raised above 200 °C to enhance the reaction rate while still enabling full loading. If partly loaded HX-BT conditions are tolerable, temperature can be chosen 50–75 K lower than needed for almost complete hydrogenation or dehydrogenation. The results obtained in this study indicate a tradeoff between maximum usage of the LOHC material and the operating temperature: e.g., loading and unloading the LOHC only between degrees of hydrogenation of 1/3 and 2/3 can allow it to operate below 200 °C but require supplying and transporting thrice as much LOHC material as for full use. Depending on the application of the LOHC technology, operating under partially loaded conditions can be feasible or even desirable.

Supporting Information

Supporting information for this article can be found under DOI: https://doi.org/10.1002/ceat.12002.

Supporting_Information: Preparation of the Pt/TiO_2 Catalyst; Deviation of Experimental Results of Hydrogenation, Conditions and Assumptions for the Computational Model, Chemical Equilibrium Theory for the Computational Model, Determination of Liquid Mixture Composition from the Computational Model, Influence of Additional Inert Gases, Optimized Geometries of HX-BT Species, Hindered Rotor Profiles.

Additionally, a spreadsheet containing the following information is available on the repository Zenodo (see https://doi.org/10.5281/zenodo.14143841):

- Ideal gas data (enthalpy, entropy, heat capacity, and Gibbs free energy) for all isomers in this study
- Relative ideal gas fractions (for $x_{H_2} \approx 1$ in the gas phase) of all HX-BT isomers for H0-BT, H6-BT, and H12-BT in chemical equilibrium for a given pressure that can be altered by the user
- Reaction equilibria for the liquid phase for given pressures that can be altered by the user
- Low-pressure data at 200 °C to produce a degree of hydrogenation similar to the values obtained in the experimental results reported in Fig. 4
- Composition-dependent data for mixture compositions of H0-BT and H12-BT in molar fraction steps of 0.2 at standard temperature

Acknowledgments

The authors acknowledge the funding by the German Federal Ministry of Education and Research (BMBF) and the Ministry of Economic Affairs, Industry, Climate Action and Energy of the State of North Rhine-Westphalia through the project HC-H2. We would like to thank the German Federal Ministry of Education and Research (BMBF) for the support within the Kopernikus project "P2X: Exploration, validation and implementation of 'Power-to-X' concepts" (FKZ 03SFK2A0-2). Special thanks to the project leader Peter Wasserscheid and the whole project team for fruitful discussions and valuable interactions. Wassja A. Kopp acknowledges funding by the Deutsche Forschungsgemeinschaft (DFG, German Research Foundation) under Germany's Excellence Strategy—Cluster of Excellence 2186 "The Fuel Science Center"—ID: 390919832. We gratefully acknowledge Eastman Chemical HTF GmbH for the supply of benzyltoluene samples. Thank you to the networking program "Sustainable Chemical Synthesis 2.0" (SusChemSys 2.0) for the support and inspiring discussions across disciplines. Special thanks to Martina Battisti, Justus Kümper, Marcus S. Lehnertz, and Natalia Simitsis for their valuable ideas and helpful support regarding the conceptual design of the experimental study. Furthermore, we thank Jan Decker, Lukas Lehmann, Frederic Thilmany, Wolf-Georg Wagner, Leander Weinelt, and Juliane Wipperfürth for their support with the experimental work as well as Sandra Brosinski, Hannelore Eschmann, Heike Fickers-Boltz, Carina Frantzen, and Björn Johnen for their support with the analytical measurements.

The authors declare no conflicts of interest.

Symbols Used

$H(T)$	[bar]	Henry constant
K	[–]	equilibrium constant
p	[bar]	pressure
T	[K]	temperature
t	[min]	time
X	[–]	number of H bonded to carrier compound
x	[–]	molar fraction
{x}	[–]	composition as set of molar fractions

Abbreviations

B3LYPD3BJ	Becke–Lee–Yang–Parr density functional with Grimme's D3 dispersion correction and Becke–Johnson damping
CCSD(T)	coupled-cluster theory with single, double, and perturbative triple excitations

DLPNO	delocalized pair natural orbital
DOH	degree of hydrogenation
H0-BT	benzyltoluene
H6-BT	partly hydrogenated benzyltoluene
H12-BT	perhydro benzyltoluene
LOHC	liquid organic hydrogen carrier
$LOHC^-$	hydrogen-lean liquid organic hydrogen carrier
$LOHC^+$	hydrogen-rich liquid organic hydrogen carrier
MR	main ring
RRHO	rigid-rotor harmonic oscillator
SI	Supporting Information
SR	side ring
TZVP	triple-zeta valence polarizable (basisset)

Data Availability Statement

Data are available on Zenodo, link to pre-publication version in the Supporting Information section.

References

[1] *Hydrogen Science and Engineering: Materials, Processes, Systems and Technology* (Eds: D. Stolten, B. Emonts), Wiley-VCH Verlag GmbH & Co. KGaA, Weinheim **2016**.

[2] R. Hren, A. Vujanović, Y. van Fan, J. J. Klemeš, D. Krajnc, L. Čuček, *Renew Sustain. Energy Rev.* **2023**, *173*, 113113. DOI: https://doi.org/10.1016/j.rser.2022.113113

[3] I. Staffell, D. Scamman, A. Velazquez Abad, P. Balcombe, P. E. Dodds, P. Ekins, N. Shah, K. R. Ward, *Energy Environ. Sci.* **2019**, *12* (*2*), 463–491. DOI: https://doi.org/10.1039/C8EE01157E

[4] P. Preuster, A. Alekseev, P. Wasserscheid, *Annu. Rev. Chem. Biomol. Eng.* **2017**, *8*, 445–471. DOI: https://doi.org/10.1146/annurev-chembioeng-060816-101334

[5] N. Brückner, K. Obesser, A. Bösmann, D. Teichmann, W. Arlt, J. Dungs, P. Wasserscheid, *ChemSusChem* **2014**, *7* (*1*), 229–235. DOI: https://doi.org/10.1002/cssc.201300426

[6] S. W. Park, J. H. Kim, J. K. Seo, *J. Mar. Sci. Eng.* **2022**, *10* (*4*), 532. DOI: https://doi.org/10.3390/jmse10040532

[7] M. Noussan, P. P. Raimondi, R. Scita, M. Hafner, *Sustainability* **2021**, *13* (*1*), 298–324. DOI: https://doi.org/10.3390/su13010298

[8] D. Teichmann, W. Arlt, P. Wasserscheid, R. Freymann, *Energy Environ. Sci.* **2011**, *4* (*8*), 2767–2773. DOI: https://doi.org/10.1039/c1ee01454d

[9] S. P. Verevkin, A. A. Samarov, V. V. Turovtsev, S. V. Vostrikov, P. Wasserscheid, K. Müller, *Appl. Sci.* **2023**, *13* (*2*), 953–975. DOI: https://doi.org/10.3390/app13020953

[10] P. M. Modisha, C. N. M. Ouma, R. Garidzirai, P. Wasserscheid, D. Bessarabov, *Energy Fuels* **2019**, *33* (*4*), 2778–2796. DOI: https://doi.org/10.1021/acs.energyfuels.9b00296

[11] F. Uhrig, J. Kadar, K. Müller, *Energy Sci. Eng.* **2020**, *8* (*6*), 2044–2053. DOI: https://doi.org/10.1002/ese3.646

[12] T. Rüde, S. Dürr, P. Preuster, M. Wolf, P. Wasserscheid, *Sustainable Energy Fuels* **2022**, *6* (*6*), 1541–1553. DOI: https://doi.org/10.1039/D1SE01767E

[13] Eastman Chemical Company, *Technical Data Sheet MARLOTHERM LH Heat Transfer Fluid*, Vol. 2021.

[14] K. Müller, K. Stark, V. N. Emel'yanenko, M. A. Varfolomeev, D. H. Zaitsau, E. Shoifet, C. Schick, S. P. Verevkin, W. Arlt, *Ind. Eng. Chem. Res.* **2015**, *54* (*32*), 7967–7976. DOI: https://doi.org/10.1021/acs.iecr.5b01840

[15] S. Biswas, K. Moreno Sader, W. H. Green, *Energy Fuels* **2023**, *37* (*22*), 17003–17012. DOI: https://doi.org/10.1021/acs.energyfuels.3c01919

[16] A. Leinweber, K. Müller, *Energy Technol.* **2018**, *6* (*3*), 513–520. DOI: https://doi.org/10.1002/ente.201700376

[17] H. Jorschick, M. Geißelbrecht, M. Eßl, P. Preuster, A. Bösmann, P. Wasserscheid, *Int. J. Hydrogen Energy* **2020**, *45* (*29*), 14897–14906. DOI: https://doi.org/10.1016/j.ijhydene.2020.03.210

[18] M. Geißelbrecht, S. Mrusek, K. Müller, P. Preuster, A. Bösmann, P. Wasserscheid, *Energy Environ. Sci.* **2020**, *13* (*9*), 3119–3128. DOI: https://doi.org/10.1039/D0EE01155J

[19] K. Müller, T. Skeledzic, P. Wasserscheid, *Energy Fuels* **2021**, *35* (*13*), 10929–10936. DOI: https://doi.org/10.1021/acs.energyfuels.1c01170

[20] Y. Kwak, J. Kirk, S. Moon, T. Ohm, Y.-J. Lee, M. Jang, L.-H. Park, C. Ahn, H. Jeong, H. Sohn, S. W. Nam, C. W. Yoon, Y. S. Jo, Y. Kim, *Energy Convers. Manage.* **2021**, *239*, 114124. DOI: https://doi.org/10.1016/j.enconman.2021.114124

[21] S. Mrusek, P. Preuster, K. Müller, A. Bösmann, P. Wasserscheid, *Int. J. Hydrogen Energy* **2021**, *7* (*59*), 15624–15634. DOI: https://doi.org/10.1016/j.ijhydene.2021.02.021

[22] J. Oh, Y. Jo, T. W. Kim, H. B. Bathula, S. Yang, J. H. Baik, Y.-W. Suh, *Appl. Catal., B* **2022**, *305*, 121061. DOI: https://doi.org/10.1016/j.apcatb.2022.121061

[23] L. Li, P. Vellayani Aravind, T. Woudstra, M. van den Broek, *Energy Convers. Manage.* **2023**, *276*, 116555. DOI: https://doi.org/10.1016/j.enconman.2022.116555

[24] S. P. Verevkin, A. A. Samarov, S. V. Vostrikov, P. Wasserscheid, K. Müller, *Hydrogen* **2023**, *4* (*1*), 42–59. DOI: https://doi.org/10.3390/hydrogen4010004

[25] D. Zakgeym, T. Engl, Y. Mahayni, K. Müller, M. Wolf, P. Wasserscheid, *Appl. Catal., A* **2022**, *639*, 118644. DOI: https://doi.org/10.1016/j.apcata.2022.118644

[26] T. W. Kim, S. H. Ko, M. Kim, Y.-W. Suh, *Adv. Powder Technol.* **2020**, *31* (*4*), 1682–1692. DOI: https://doi.org/10.1016/j.apt.2020.02.012

[27] S. P. Verevkin, S. V. Vostrikov, A. Leinweber, P. Wasserscheid, K. Müller, *Fuel* **2023**, *335*, 126618. DOI: https://doi.org/10.1016/j.fuel.2022.126618

[28] G. P. Moss, *Pure Appl. Chem.* **1996**, *68* (*12*), 2193–2222. DOI: https://doi.org/10.1351/pac199668122193

[29] M. Lal, F. L. Swinton, *Trans. Faraday Soc.* **1967**, *63*, 1596–1602. DOI: https://doi.org/10.1039/TF9676301596

[30] L. Foppa, J. Dupont, *Chem. Soc. Rev.* **2015**, *44* (*7*), 1886–1897. DOI: https://doi.org/10.1039/c4cs00324a

[31] W. Steele, *J. Chem. Thermodyn.* **1995**, *27* (*6*), 671–678. DOI: https://doi.org/10.1006/jcht.1995.0068

[32] R. D. Chirico, W. V. Steele, *J. Chem. Eng. Data* **2005**, *50* (*3*), 1052–1059. DOI: https://doi.org/10.1021/je050034s

[33] A. L. L. East, L. Radom, *J. Chem. Phys.* **1997**, *106* (*16*), 6655–6674. DOI: https://doi.org/10.1063/1.473958

[34] J. Zheng, T. Yu, E. Papajak, I. M. Alecu, S. L. Mielke, D. G. Truhlar, *Phys. Chem. Chem. Phys.* **2011**, *13* (*23*), 10885–10907. DOI: https://doi.org/10.1039/c0cp02644a

[35] P. Vansteenkiste, V. van Speybroeck, G. B. Marin, M. Waroquier, *J. Phys. Chem. A* **2003**, *107* (*17*), 3139–3145. DOI: https://doi.org/10.1021/jp027132u

[36] X. Chen, C. H. Gierlich, S. Schötz, D. Blaumeiser, T. Bauer, J. Libuda, R. Palkovits, *ACS Sustain. Chem. Eng.* **2021**, *9*

(*19*), 6561–6573. DOI: https://doi.org/10.1021/acssuschemeng.0c09048
[37] B. Bong, C. Mebrahtu, D. Jurado, A. Bösmann, P. Wasserscheid, R. Palkovits, *ACS Eng. Au* **2024**, *4* (*3*), 359–367. DOI: 10.1021/acsengineeringau.4c00003
[38] A. D. Becke, *J. Chem. Phys.* **1993**, *98* (*7*), 5648–5652. DOI: https://doi.org/10.1063/1.464913
[39] A. D. Becke, *J. Chem. Phys.* **1992**, *96* (*3*), 2155–2160. DOI: https://doi.org/10.1063/1.462066
[40] A. D. Becke, *J. Chem. Phys.* **1992**, *97* (*12*), 9173–9177. DOI: https://doi.org/10.1063/1.463343
[41] C. Lee, W. Yang, R. G. Parr, *Phys. Rev. B: Condens. Matter Mater. Phys.* **1988**, *37* (*2*), 785–789. DOI: https://doi.org/10.1103/PhysRevB.37.785
[42] S. Grimme, S. Ehrlich, L. Goerigk, *J. Comput. Chem.* **2011**, *32* (*7*), 1456–1465. DOI: https://doi.org/10.1002/jcc.21759
[43] A. Schäfer, C. Huber, R. Ahlrichs, *J. Chem. Phys.* **1994**, *100* (*8*), 5829–5835. DOI: https://doi.org/10.1063/1.467146
[44] F. Weigend, R. Ahlrichs, *Phys. Chem. Chem. Phys.* **2005**, *7* (*18*), 3297–3305. DOI: https://doi.org/10.1039/b508541a
[45] K. K. Irikura, R. D. Johnson, R. N. Kacker, *J. Phys. Chem. A* **2005**, *109* (*37*), 8430–8437. DOI: https://doi.org/10.1021/jp052793n
[46] J. P. Merrick, D. Moran, L. Radom, *J. Phys. Chem. A* **2007**, *111* (*45*), 11683–11700. DOI: https://doi.org/10.1021/jp073974n
[47] M. J. Frisch, G. W. Trucks, H. B. Schlegel, G. E. Scuseria, M. A. Robb, J. R. Cheeseman, G. Scalmani, V. Barone, G. A. Petersson, H. Nakatsuji, X. Li, M. Caricato, A. V. Marenich, J. Bloino, B. G. Janesko, R. Gomperts, B. Mennucci, H. P. Hratchian, J. V. Ortiz, A. F. Izmaylov, J. L. Sonnenberg, F. Ding Williams, F. Lipparini, F. Egidi, J. Goings, B. Peng, A. Petrone, T. Henderson, D. Ranasinghe, V. G. Zakrzewski, J. Gao, N. Rega, G. Zheng, W. Liang, M. Hada, M. Ehara, K. Toyota, R. Fukuda, J. Hasegawa, M. Ishida, T. Nakajima, Y. Honda, O. Kitao, H. Nakai, T. Vreven, K. Throssell, J. A. Montgomery Jr., J. E. Peralta, F. Ogliaro, M. J. Bearpark, J. J. Heyd, E. N. Brothers, K. N. Kudin, V. N. Staroverov, T. A. Keith, R. Kobayashi, J. Normand, K. Raghavachari, A. P. Rendell, J. C. Burant, S. S. Iyengar, J. Tomasi, M. Cossi, J. M. Millam, M. Klene, C. Adamo, R. Cammi, J. W. Ochterski, R. L. Martin, K. Morokuma, O. Farkas, J. B. Foresman, D. J. Fox, *Gaussian 16 Rev. C.01*, Wallingford, CT **2016**.
[48] A. Ghysels, T. Verstraelen, K. Hemelsoet, M. Waroquier, V. van Speybroeck, *J. Chem. Inf. Model.* **2010**, *50* (*9*), 1736–1750. DOI: https://doi.org/10.1021/ci100099g
[49] W. A. Kopp, M. L. Mödden, N. Viswanathan, G. Rath, K. Leonhard, *Phys. Chem. Chem. Phys.* **2023**, *25* (*16*), 11316–11323. DOI: https://doi.org/10.1039/D2CP03907A
[50] F. Neese, E. F. Valeev, *J. Chem. Theory Comput.* **2011**, *7* (*1*), 33–43. DOI: https://doi.org/10.1021/ct100396y
[51] D. G. Liakos, M. Sparta, M. K. Kesharwani, J. M. L. Martin, F. Neese, *J. Chem. Theory Comput.* **2015**, *11* (*4*), 1525–1539. DOI: https://doi.org/10.1021/ct501129s
[52] L. C. Kröger, M. Döntgen, D. Firaha, W. A. Kopp, K. Leonhard, *Proc. Combust. Inst.* **2019**, *37* (*1*), 275–282. DOI: https://doi.org/10.1016/j.proci.2018.06.056
[53] F. Neese, *Wiley Interdiscip. Rev.: Comput. Mol. Sci.* in press. DOI: https://doi.org/10.1002/wcms.1606
[54] P. Linstrom, *NIST Chemistry WebBook, NIST Standard Reference Database 69*, National Institute of Standards and Technology **1997**.
[55] J. A. Manion, *J. Phys. Chem. Ref. Data* **2002**, *31* (*1*), 123–172. DOI: https://doi.org/10.1063/1.1420703
[56] D. A. Pittam, G. Pilcher, *J. Chem. Soc., Faraday Trans. 1* **1972**, *68*, 2224. DOI: https://doi.org/10.1039/F19726802224
[57] M. V. Roux, M. Temprado, J. S. Chickos, Y. Nagano, *J. Phys. Chem. Ref. Data* **2008**, *37* (*4*), 1855–1996. DOI: https://doi.org/10.1063/1.2955570
[58] A. Klamt, *J. Phys. Chem.* **1995**, *99* (*7*), 2224–2235. DOI: https://doi.org/10.1021/j100007a062
[59] A. Klamt, V. Jonas, T. Bürger, J. C. W. Lohrenz, *J. Phys. Chem. A* **1998**, *102* (*26*), 5074–5085. DOI: https://doi.org/10.1021/jp980017s
[60] A. Klamt, F. Eckert, W. Arlt, *Annu. Rev. Chem. Biomol. Eng.* **2010**, *1*, 101–122. DOI: https://doi.org/10.1146/annurev-chembioeng-073009-100903
[61] BIOVIA, Dassault Systèmes, *BIOVIA COSMOconf 2022*, San Diego: Dassault Systèmes, **2022**.
[62] BIOVIA, Dassault Systèmes, *BIOVIA COSMOtherm 2022*, San Diego: Dassault Systèmes, **2022**.
[63] T. Nevolianis, N. Wolter, L. F. Kaven, L. Krep, C. Huang, A. Mhamdi, A. Mitsos, A. Pich, K. Leonhard, *Ind. Eng. Chem. Res.* **2023**, *62* (*2*), 893–902. DOI: https://doi.org/10.1021/acs.iecr.2c03291
[64] P. W. Atkins, P. Julio de, *Atkins' Physical Chemistry*, 10th ed., Oxford University Press, Oxford **2015**.
[65] C. Wulf, P. Zapp, *Int. J. Hydrogen Energy* **2018**, *43* (*26*), 11884–11895. DOI: https://doi.org/10.1016/j.ijhydene.2018.01.198
[66] R. Dickson, M. S. Akhtar, A. Abbas, E. D. Park, J. Liu, *Green Chem.* **2022**, *24* (*21*), 8484–8493. DOI: https://doi.org/10.1039/D2GC02079C

